Role of pressure solution in the formation of bedding-parallel calcite veins in an immature shale (Cretaceous, southern UK)

QINGFENG MENG†, JOHN HOOKER & JOE CARTWRIGHT

Department of Earth Sciences, University of Oxford, South Parks Road, Oxford, OX1 3AN, UK

Abstract – Bedding-parallel fibrous calcite veins in black shales (Cretaceous, southern UK) were investigated using a combined field, stable isotopic geochemistry, petrographic and crystallographic method to examine their formation mechanism. Calcite veins occur in all shale beds and are most abundant in the bituminous shales of the Chief Beef Beds. The calcite fibres in these veins exhibit either an antitaxial fibre growth with curvy stylolites as the median zone, or a predominantly syntaxial, upwards growth. The calcite veins range from –0.49 to 1.78 ‰ of $\delta^{13}C$ values, and –6.53 to –0.03 ‰ of $\delta^{18}O$ values, which are both similar to those of their host shales. Our petrographic observations demonstrate that subhorizontal and interconnecting microstylolite networks commonly occur within the calcite veins. Equant calcite grains in the median zones exhibit indenting, truncating and also interpenetrating grain contacts. It is interpreted that the fibrous calcite veins were sourced by neomorphic calcite from their host shales, with evidence from the $\delta^{13}C$ signatures, pressure-solution features (stylolites, microstylolites and grain contact styles) and embedded fossil ghosts within the veins. The diagenetic fluids, from which calcite was precipitated, were a mixing of the original seawaters and ^{18}O-depleted meteoric waters. Development of bedding-parallel calcite veins is considered to have been enhanced by pressure solution as a positive feedback mechanism, which was facilitated by the overburden pressure as the maximum principal stress. Calcite fibres, with a predominant subvertical c-axis orientation, exhibit a displacive growth in porous shales and a replacive growth at vein-limestone contacts. This study highlights the critical role of pressure solution in the formation of bedding-parallel calcite veins during burial and diagenesis of immature black shales.

Keywords: pressure solution, beef, shale, c-axis.

1. Introduction

Pressure solution is a deformation process by which grains dissolve at intergranular or intercrystalline contacts under high stress in an aqueous solution (Thomson, 1959; Weyl, 1959; Rutter & Elliott, 1976; Fletcher & Pollard, 1981; Rutter, 1983; Tada & Siever, 1989). Such a process is caused by a higher solubility under non-hydrostatic stresses at grain-to-grain contacts. Two common types of pressure solution have been recognized: intergranular pressure solution and stylolitization (Houseknecht, 1984; Tada & Siever, 1989; Dewers & Ortoleva, 1990; Bjorkum, 1996). Intergranular pressure solution, as a diagenetic mechanism, contributes significantly to porosity reduction and compaction, serving as the agent of intergranular compaction and a source of cement (e.g. Sibley & Blatt, 1976; Houseknecht, 1984, 1988; Tada, Maliva & Siever, 1987; Lehner, 1995; Renard, Ortoleva & Gratier, 1997; Renard, Gratier & Jamtveit, 2000; Yasuhara, Elsworth & Polak, 2003). Stylolites can be recognized by serrated surfaces within the rock mass, where insoluble minerals, such as clay, iron minerals and organic matter, are concentrated (Park & Schot, 1968). Based on their morphology, stylolites can be subdivided into several types with varied amplitudes of

offset, column frequency, peak angles, orientations and connectivities (Fig. 1) (Koehn *et al*. 2016). Stylolites have been regarded as an important cement source, especially for late diagenetic calcite spar (Oldershaw & Scoffin, 1967; Finkel & Wilkinson, 1990; Rezaee & Tingate, 1997; Worden, Oxtoby & Smalley, 1998; Baron & Parnell, 2007; Koehn *et al*. 2016). Stylolites can prevent fluid flow (Heap *et al*. 2014), or serve as conduits for fluid flow (Carozzi & Von Bergen, 1987; Braithwaite, 1989).

It has been recognized that bedding-parallel fibrous veins (or 'beef') are common in black shales in sedimentary basins worldwide, where they are often taken as evidence for high pore fluid pressures (Cobbold *et al*. 2013). The characteristic feature of such veins is that they consist of parallel-aligned crystals with a maximum length of several centimetres, and exhibit a fibrous texture (Bons, 2000; Bons, Elburg & Gomez-Rivas, 2012). Multiple mechanisms have been proposed to explain the genesis of these veins (Table 1); however, the debate still remains. The key questions to discuss mainly include: (1) the mechanism that triggered the initiation of bedding-parallel veins; and (2) the origin of the fibrous habit of crystals and the driving force for vein expansion.

In this paper we report a field, isotopic, petrographic and crystallographic study of the bedding-parallel calcite veins in the Stair Hole Member exposed in

†Author for correspondence: meng.qingfeng@hotmail.com

Table 1. Summary of the proposed formation mechanisms of bedding-parallel mineral veins.

| Mechanism		References
Over-pressure	Oil primary migration	Stoneley (1983); Lindgreen (1985); Parnell & Carey (1995); Parnell *et al*. (2000); Suchy *et al*. (2002); Rodrigues *et al*. (2009); Zanella, Cobbold & Boassen (2015)
	Generation of methane gas	Jowett (1987); Rukin (1990); Evans (1995); Meng, Hooker & Cartwright, (2017*a*)
	Seepage force	Cobbold & Rodrigues (2007); Zanella, Cobbold & De Veslud (2014); Maher, Ogata & Braathen (2016)
	Tectonic compression	Shearman *et al*. (1972); Cosgrove (2001); Vannucchi (2001); Machel (1985); Meng, Hooker & Cartwright (2017*b*)
	Mineral dewatering	Fitches *et al*. (1986); Parnell, Ansong & Veale (1994); Hara & Hisada (2007)
	External fluid injection	Al-Aasm, Coniglio & Desrochers (1995); Hillier & Cosgrove (2002); Li *et al*. (2013)
Force of crystallization		Taber (1918); Watts (1978); Means & Li (2001); Wiltschko & Morse (2001); Hilgers & Urai (2005)
Shear fracturing		Selles-Martinez (1994); Conybeare & Shaw (2000); Jamison (2013)
Strata dissolution and collapse		Gustavson, Hovorka & Dutton (1994)
Sediment unloading		El-Tabakh & Warren (1998)
Flexural-slip folding		Jessell, Willman & Gray (1994); Fowler (1996); Fowler & Winsor (1997); Koehn & Passchier (2000)
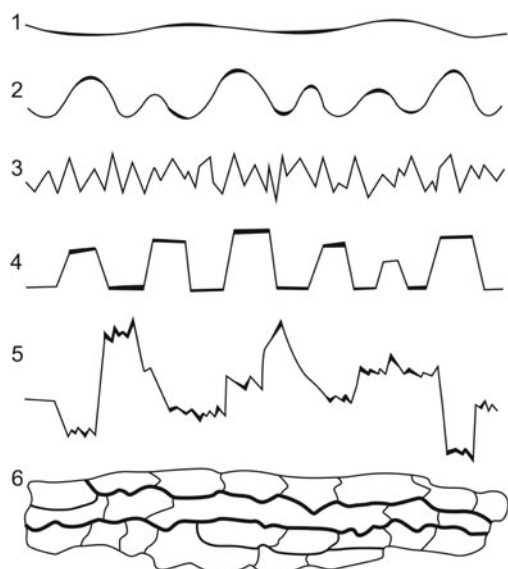
Figure 1. Classification of stylolites: 1, smooth trace; 2, wavy columns; 3, sharp peaks; 4, rectangular columns; 5, composite texture; 6, fitted fabric. Modified from Park & Schot (1968), Buxton & Sibley (1981) and Guzzetta (1984).

Dorset, southern UK. The work extends the original study of El-Shahat & West (1983) on the diagenesis of the Purbeck Formation by extending the investigation of the calcite veins to encompass their stratigraphic distribution, morphology, size, stable isotope geochemistry, petrography and c-axis crystallography. This paper aims to provide new evidence for: (1) the diagenetic environment for fibrous calcite veins; (2) the vein formation mechanism; and (3) the mutual interplay between vein fabrics and their growth processes. The results presented in this study suggest that there is a positive feedback between pressure solution and the development of bedding-parallel calcite veins during chemical compaction of the host fossiliferous sediments, when the thermal maturity of organic matter is not high enough to generate hydrocarbons. This study also raises the important possibility

that the classical views regarding the formation mechanism of bedding-parallel veins in shale may need to be re-evaluated.

2. Geological background

The study area is located on the coastal area of the Durlstone Bay, Dorset, southern UK (Fig. 2a). The cliffs expose 119 m thick alternating limestones and shales of the Purbeck Group (Upper Jurassic – Lower Cretaceous) (Fig. 2b, c). The beds are NWW–SEE-striking and gently dipping towards north at 10°. The lower boundary of the Purbeck is defined by the first occurrence of finely laminated, ostracod-rich limestones above the more massive, shelly limestones of the Portland Group (Horton, 1995). The overlying Wealden Group can be identified by the occurrence of sandy mudstones above the last occurrence of limestones of the Purbeck Group (Stewart *et al*. 1991; Robinson & Hesselbo, 2004). The thin-bedded limestones and calcareous shales of the Purbeck Group have been considered as lagoonal deposits, which are richly fossilifeous, especially bivalves (Andrews & Walton, 1990; Stewart *et al*. 1991; Radley, Barker & Munt, 1998). There have been multiple rapid salinity fluctuations of the Purbeck Group. This is represented by a progressive change from evaporites of hypersaline origin in lower Purbeck strata to alternating freshwater, brackish and marine in the middle Purbeck strata to dominantly freshwater with influx of land-derived clastics in the upper Purbeck strata (Stewart *et al*. 1991; Schnyder *et al*. 2006; Radley, 2009). The middle part of the Purbeck Group has been extensively studied because the unlithified shell limestones are best developed within this interval (El-Shahat & West, 1983; Clements, 1993; Westhead & Mather, 1996). The most common bivalve deposits of the Purbeck Group consist of disarticulated valves of brackish-water bivalves. The unlithified shell beds typically contain white aragonite shells, whereas the lithified shell beds are
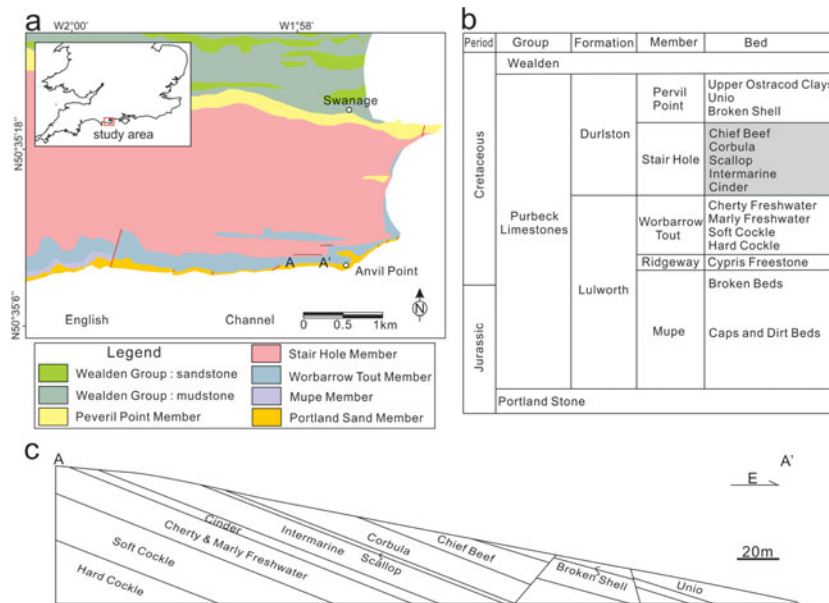
Figure 2. (Colour online) (a) Geological map of the study area in southern Dorset, UK. Modified from British Geological Survey (2000). (b) Simplified stratigraphic column of the Purbeck Group of the Wessex Basin. Modified from Hopson, Wilkinson & Woods (2008). (c) Cross-section of the cliffs exposed on the Durlston Bay along line A–A′ (see location in Fig. 2a).

composed of biosparites or biosparrudites with varying content of aragonite retained (El-Shahat & West, 1983). Bedding-parallel calcite veins are commonly present in the Stair Hole Formation of the middle part of the Purbeck Group (El-Shahat & West, 1983; Westhead & Mather, 1996). The Stair Hole Formation can be further subdivided into five beds with different lithologies and degrees of lithification (Fig. 2b) (Westhead & Mather, 1996).

3. Methods

An integrated research method of field, optical and SEM petrography and crystallography, as well as stable isotope geochemistry, was used to study the bedding-parallel veins. Field investigation mainly focused on the distribution, geometry and abundance of calcite veins and their host rock lithologies. Calcite veins and their host rocks were sampled for carbon and oxygen isotope measurements, to derive information on the carbonate source, diagenetic fluid and environment. The measurements were conducted using Thermo MAT 253 mass spectrometers at the Stable Isotope Geochemistry Laboratory of the Open University, following the procedure described by Meng, Hooker & Cartwright (2017a). Oxygen ($\delta^{18}O$) and carbon ($\delta^{13}C$) isotopes were obtained at precision better than ±0.06 and ±0.05, respectively. Thin-sections of representative rock samples of calcite veins and surrounding rocks were cut perpendicular to bedding. We used a polarized light microscope and a FEI Quanta 650 scanning electron microscope (SEM) to observe vein microstructures, mineral compositions and diagenetic alternations of the host rocks. We also used the electron backscatter diffraction (EBSD) technique to quantitat-

ively measure crystallographic preferred orientations (CPO) (Humphreys, 2004) and sizes of calcite crystals in the vein samples, so that the information of crystal growth and palaeostress states could be revealed (Meng, Hooker & Cartwright, 2018). The polished thin-sections were mounted on a tilted SEM stage at 70° from the horizontal, with the vein walls being parallel to the x-axis of the stage. The measurement was conducted at 20 kV accelerating voltage, and a working distance of 10 mm from the EBSD detector. Electron beam scattering patterns were automatically collected using the Aztec software package for identification of the crystal orientations. The microstructural maps were then generated to spatially describe the crystal lattice orientations. The c-axis orientations of some selected crystals were plotted as lower-hemisphere, equal-area stereographic projections using the HKL Channel 5 software, which allows a comparison between these crystals.

4. Field observations

4.a. Vein distribution

Bedding-parallel, fibrous calcite veins were found in all the shale-containing beds of the Stair Hole Formation, except the Scallop Bed (Table 2). Fibrous calcite veins are prevalent in the Chief Beef Beds, occurring in every shale bed. They are most abundant in Bed 219 (Fig. 3a–e), which consists of bituminous shales of thickness 55 cm. The shales are rich in iron and original skeletal aragonite. The bedding-parallel veins are intensively developed and tightly clustered. Fifty-five veins occur along a linear scanline normal to bedding, with an average spacing of 6.35 mm (spacing is here defined as the thickness of shale between two

Table 2. Characteristics of the beds of the Stair Hole Formation exposed in the study area.

| Bed name	Bed number	Thickness (m)	Lithology	Fossil	Vein occurrence
Chief Beef	190–219	8.3	Limestone (mainly biosparrudite) and organic-rich shale	Bivalve	Yes
Corbula	154–189	10.9	Limestones and carbonaceous shales	Gastropod and bivalve	Yes
Scallop	145–153	1.6	Biosparrudite	Bivalve	No
Intermarine	112–144	15.5	Biosparrudite with some pyritic shales	Bivalve	Yes
Cinder	111	2.9	Blue-grey biomicrites	Oyster	Yes
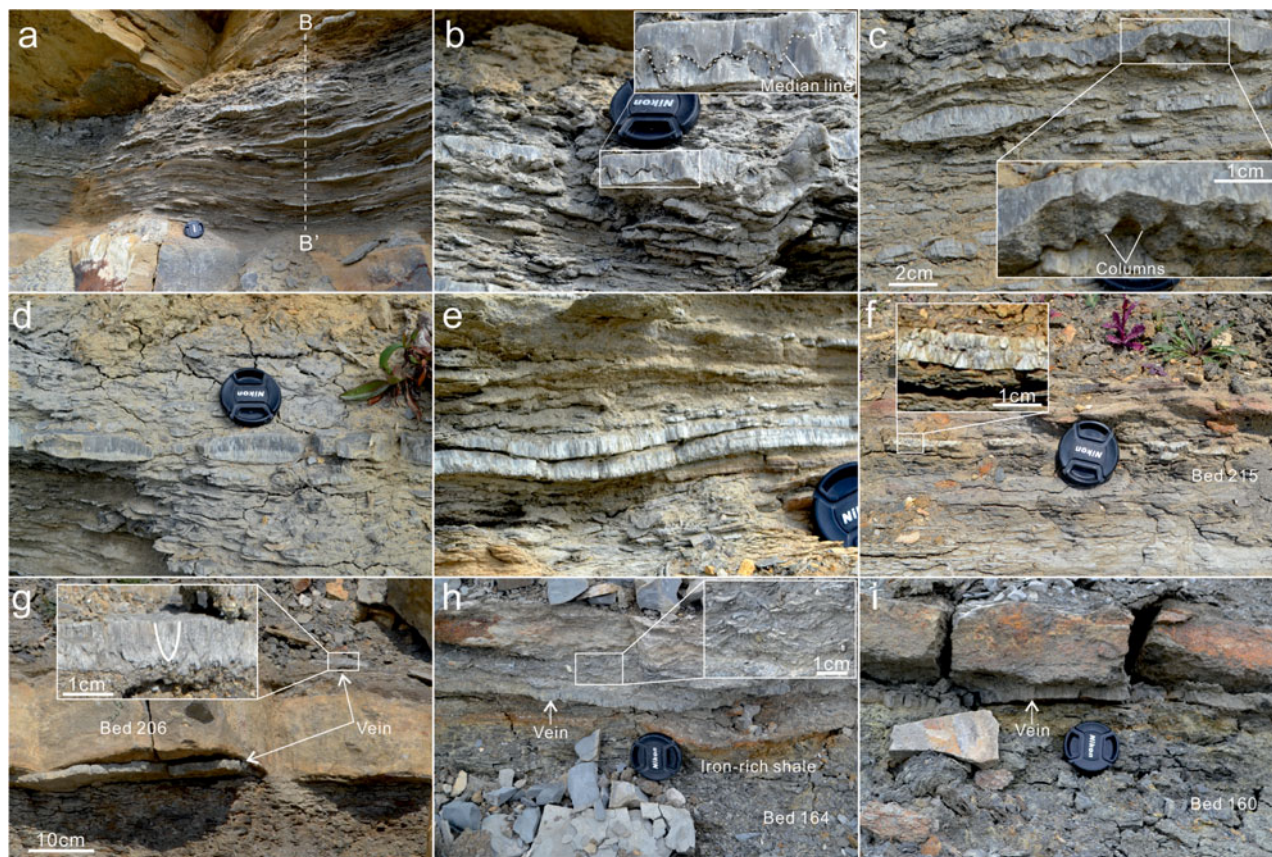
Figure 3. (Colour online) Field photographs showing the distribution of bedding-parallel calcite veins in beds (a–e) 219, (f) 215 and (g) 207 of the Chief Beef Bed; and (h) 164 and (i) 160 of the Corbula Bed. (a) Tightly spaced subhorizontal veins. (b) A 1.7 cm thick vein with a curvy median zone filled with dark host-rock inclusions. (c) Two neighbouring thick veins: the upper vein exposes the stylolite surface of its upper part and the enlarged area shows the forest of multiple columns; the lower vein exhibits a lenticular geometry with tapering tips. (d) Multiple veins exhibit rounded ends, with a geometry resembling boudinage structures. (e) Two neighbouring veins with a vertical spacing of only several millimetres. (f) A vein exhibiting a central medina zone and two fibrous parts. (g) Calcite veins above and beneath Bed 206. The enlarged area shows the upwards syntaxial growth of calcite fibres in the vein, indicated by the gradual coarsening of crystal aggregates. (h) A vein in iron- and shell-rich shales. The enlarged area shows the prevalent aragonitic shells above the vein. (i) A vein in iron-rich shales beneath the lower plane of Bed 165. Camera cap is 5.2 cm in diameter.

neighbouring veins) (Fig. 4). Vein sizes vary over the range 0.2–2.8 cm in thickness, and 1–2 cm to tens of metres in length. Other shale beds of the Chief Beef Bed contain only one or two calcite veins (Fig. 3f–i). The veins lie either in the central part of the beds, or more commonly close to the neighbouring limestone beds (<10 cm). For example, two veins in Beds 205 and 207 were found to bound their host shales and a limestone bed (Bed 206) (Fig. 3g).

Persistent bedding-parallel calcite veins with a maximum thickness of 1.3 cm were observed in Beds 160 and 164 of the Corbula Bed (Fig. 3h, i). This bed also contains abundant aragonitic bivalves and gastropods,

which have not been lithified. The only shale bed of the Intermarine Bed, Bed 130 consists of a 1.5 cm thick calcite vein and prevalent shell debris. Three to four closely spaced calcite veins were found at the more argillaceous, uppermost part of the Cinder Bed (Bed 111), which contains bluish, grey shelly limestone with oysters. The veins are persistent in length and vary over the range 2–5 mm in thickness.

4.b. Morphology

The calcite veins are either tabular-shaped and persistent in length, or are spindle-shaped with
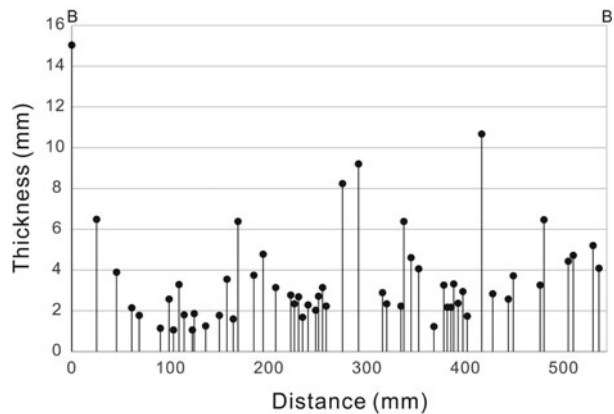
Figure 4. Vein thickness distribution along line B–B′. See location in Figure 3a.

conspicuous tips (Fig. 3c). Some vein tips sharply taper, whereas many others exhibit blunt or even rounded tips (Fig. 3d). The veins consist of closely packed vertical fibres, which are approximately normal to vein-walls. Some calcite veins contain a median zone that bounds the upper and lower fibres (Fig. 3f). The median zones are either straight or curvy, and are mostly nearer to the lower vein-walls, that is, the upper fibres are predominantly longer than the lower fibres. The curvy median zones exhibit characteristic features of stylolites (Fig. 3c), with a maximum column amplitude of 8 mm. The crowns of individual columns are commonly curvy, and the peaks are rather blunt. Three-dimensional shapes of stylolites are occasionally weathered out, exposing a forest of columns and matching pits normal to the planes of the stylolites. Median zones are commonly absent from many calcite veins (Fig. 3g). In such veins, calcite fibres become coarser towards the upper vein-walls, exhibiting a syntaxial, upwards growth.

Vein surfaces are commonly irregular. The rugosity of vein planes can be attributed to the variable degrees of fibre protrusions into the host rocks. For example, the uppermost calcite vein of Bed 219 (Chief Beef) with rough planes results in the corresponding irregularity in the contact with the limestone of Bed 220 (Broken Shell) (Fig. 5a). This demonstrates that the longer fibres in the vein have protruded into the limestone, causing a differential compaction of the limestone. It is also observed that thin calcite veins at the top of the Cinder Bed contain numerous bivalve residues on vein surfaces (Fig. 5b). The fossil morphologies are rather intact, which contributes to the irregular surface geometry of vein planes.

5. Stable isotope signatures

The $\delta^{13}C$ values of the calcite veins from the Chief Beef Bed vary from –0.49 to 1.78‰ PDB (Fig. 6). Coupled with their $\delta^{18}O$ compositions, the veins can be subdivided into two groups (Fig. 7). Veins of group I mostly occur in the upper part of this bed and exhibit positive $\delta^{13}C$ values ranging from 1.11 to 1.78‰ PDB. Group II are located in the lower part of this bed and have negative values ranging from –0.49 to –0.30‰ PDB. The $\delta^{18}O$ values of both groups are between –6.74 and –5.47‰ PDB, and are generally overlapped and undifferentiable.

The limestones of the Chief Beef Bed exhibit varied stable isotope compositions, –0.90 to 1.85‰ PDB of $\delta^{13}C$ values, and –6.53 to –0.03‰ PDB of $\delta^{18}O$ values (Fig. 6). The $\delta^{13}C$ compositions of the limestones are similar to those of calcite veins; however, their $\delta^{18}O$ compositions cross a much wider range. The anomalies of $\delta^{18}O$ values occur in Beds 192, 194 and 198, which all consist of unlithified aragonitic bivalves, with $\delta^{18}O$ values ranging from –0.54 to –0.03‰ PDB. The limestone beds with $\delta^{18}O$ values from –4.00 to –3.00‰ PDB consist of ostracod biosparite limestone. The biosparrudite limestone beds fall into a narrow range of $\delta^{18}O$ values from –5.15 to –5.37‰ PDB. The $\delta^{18}O$ values of other types of limestones are overlapped between –6.53 and –4.43‰ PDB.

The shale beds of the Chief Beef Bed exhibit a narrower range of stable isotope compositions than the
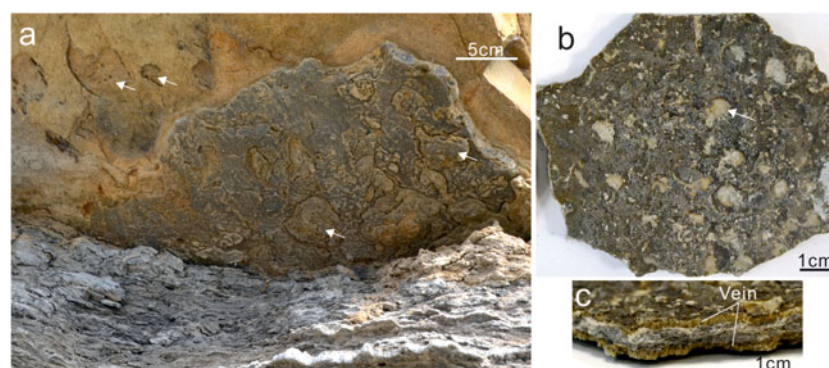

Figure 5. (Colour online) Surface morphology of calcite veins from beds (a) 219 and (b, c) 111. (a) The non-smooth lower surface of the calcite vein beneath the limestones of Bed 220. The arrows point to the circular depressions in the lower plane of the limestone bed, which could correspond to the circular protrusions in vein planes. (b) The upper surface of a thin vein. The arrow points to a typical circular depression which resulted from shell remains. (c) Cross-section view of the sample in (b). The two thin veins are bounded by biosparrudite limestone.
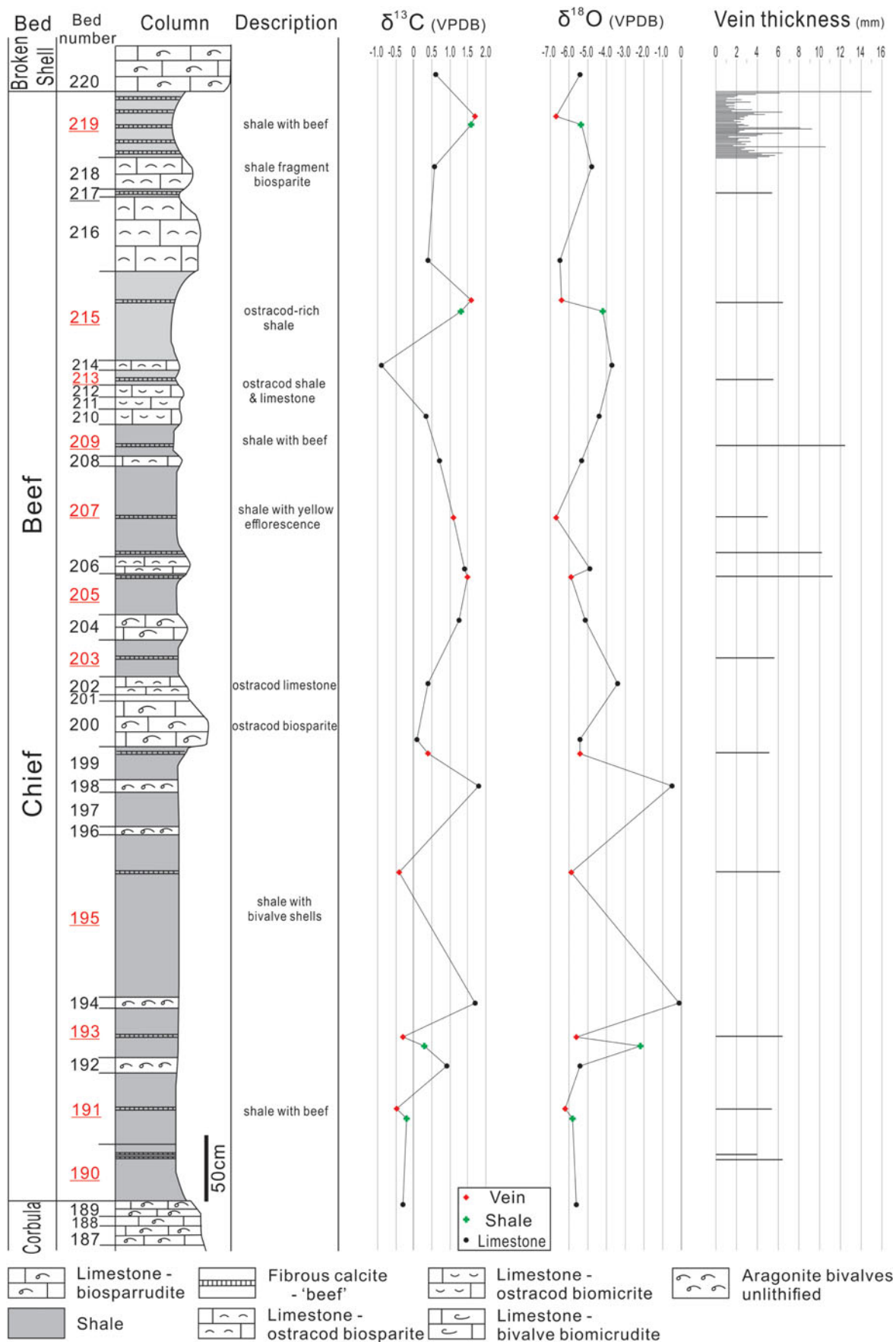
Figure 6. (Colour online) Stratigraphic column of the Chief Beef Bed with lithological descriptions, carbon and oxygen isotope compositions of veins, shales and limestones, and also vein thickness. The beds containing calcite veins are highlighted by underlining bed numbers. The column is modified from El-Shahat & West (1983).
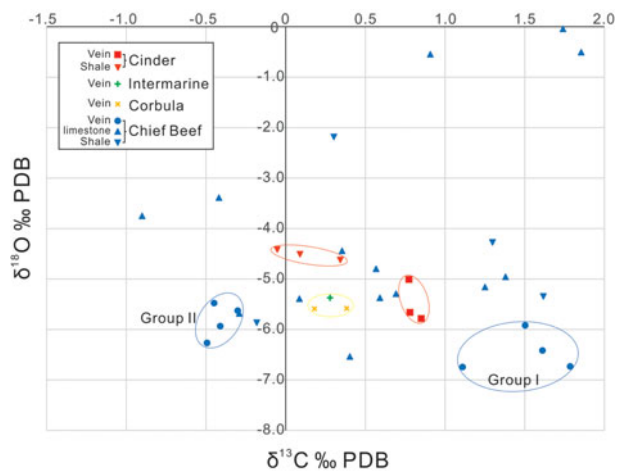
Figure 7. (Colour online) Plot of carbon versus oxygen isotope values of calcite veins, shales and limestones from the Stair Hole Member.

limestone beds, with $\delta^{13}C$ values between –0.18 and 1.61‰ PDB, and $\delta^{18}O$ values between –5.86 and –2.18‰ PDB. An anomaly appears in Bed 193, which is adjacent to two unlithified bivalve beds and exhibits a less negative $\delta^{18}O$ of –2.18‰ PDB.

The other calcite vein samples from the Corbula, Intermarine and Cinder Beds all have positive $\delta^{13}C$ values ranging from 0 to 1‰ PDB, and $\delta^{18}O$ values ranging from –6 to –5‰ PDB. It is notable that the calcite veins from the Cinder Bed exhibit higher $\delta^{13}C$ and lower $\delta^{18}O$ values than those of their host rocks (Fig. 8).

6. Petrography

6.a. Microtextures

The curvy median zones of stylolites in individual calcite veins consists of multiple columns with a height ranging from 0.2 to 2.1 mm, and a frequency of 0.7 mm^{-1} (Fig. 9). The stylolites mainly contain insoluble clay minerals, organic matter and pyrite microcrystals. The thickness of the stylolites varies from several microns to 0.6 mm. The original structure of fine laminations has largely been retained (Fig. 9b, c), which are parallel to the contacting flanks of columns. Plastic deformation and shear fractures commonly occur in the clay aggregates.

Calcite occurs in two major forms in the veins, either as equant, small crystals, or as larger fibres with a much higher aspect (length/width) ratio. Here, small crystals are defined as those with an area size less than 10^4 μm^2. The small calcite crystals are predominantly concentrated along the stylolites, especially at the crowns of individual columns. These crystals have an average area size of 2368 μm^2, and an average aspect ratio of 3.3. The larger calcite crystals have an average area size of 29 443 μm^2 and an average aspect ratio of 7.0, indicating that larger crystals tend to exhibit a lenticular or fibrous morphology. The calcite fibres are parallel, tightly aligned with the long axes lying vertically. The lower parts of single veins are generally pure in composition, whereas the upper parts contain numerous scattered inclusion patches of clay grains, pyrite and also organic matter. The upper walls of the veins also often exhibit a greater irregularity than the lower walls (Fig. 9a).

Ghosts of bivalve fragments are commonly observed to be embedded within the fibrous veins (Fig. 9d, e). The bivalve fragments are commonly flat or curved. Their length ranges from 20 to 150 μm, and thickness from 1 to 4 μm. The bivalve fragments mostly lie parallel to bedding; however, some fragments are oblique to bedding at an angle of up to 55°. Clay aggregates are commonly associated with the bivalve fragments. The clay aggregates, with a thickness of 5–80 μm, predominantly lie below the bivalve fragments. Fibrous calcite crystals, which lie above the bivalve fragments, are rooted in the fragments, with little host-rock inclusions between them.

A crystalline mosaic of small, equant calcite crystals were also found filling the moulds of skeletal fragments as a sparry calcite cement (Fig. 10). The crystal morphologies are similar to those in the stylolites of fibrous veins. Individual crystals are discernible with the long dimension ranging over 5–300 μm. The morphologies of the skeletal fragments are well preserved, possibly because the cementation process predates mechanical compaction, so that crushing of the shell fragments has been avoided. Such sparry calcite cements have been suggested to be the result of neomorphism of aragonite during diagenesis, and represent an important manifestation of porosity reduction (El-Shahat & West, 1983).
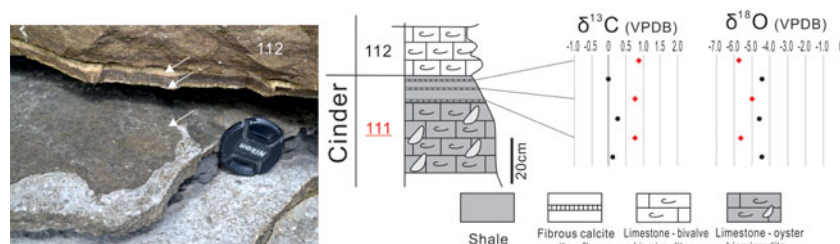

Figure 8. (Colour online) The calcite veins lying on the topmost part of Bed 111 of the Cinder Bed, and the carbon and oxygen isotope compositions of the veins and their host rocks.
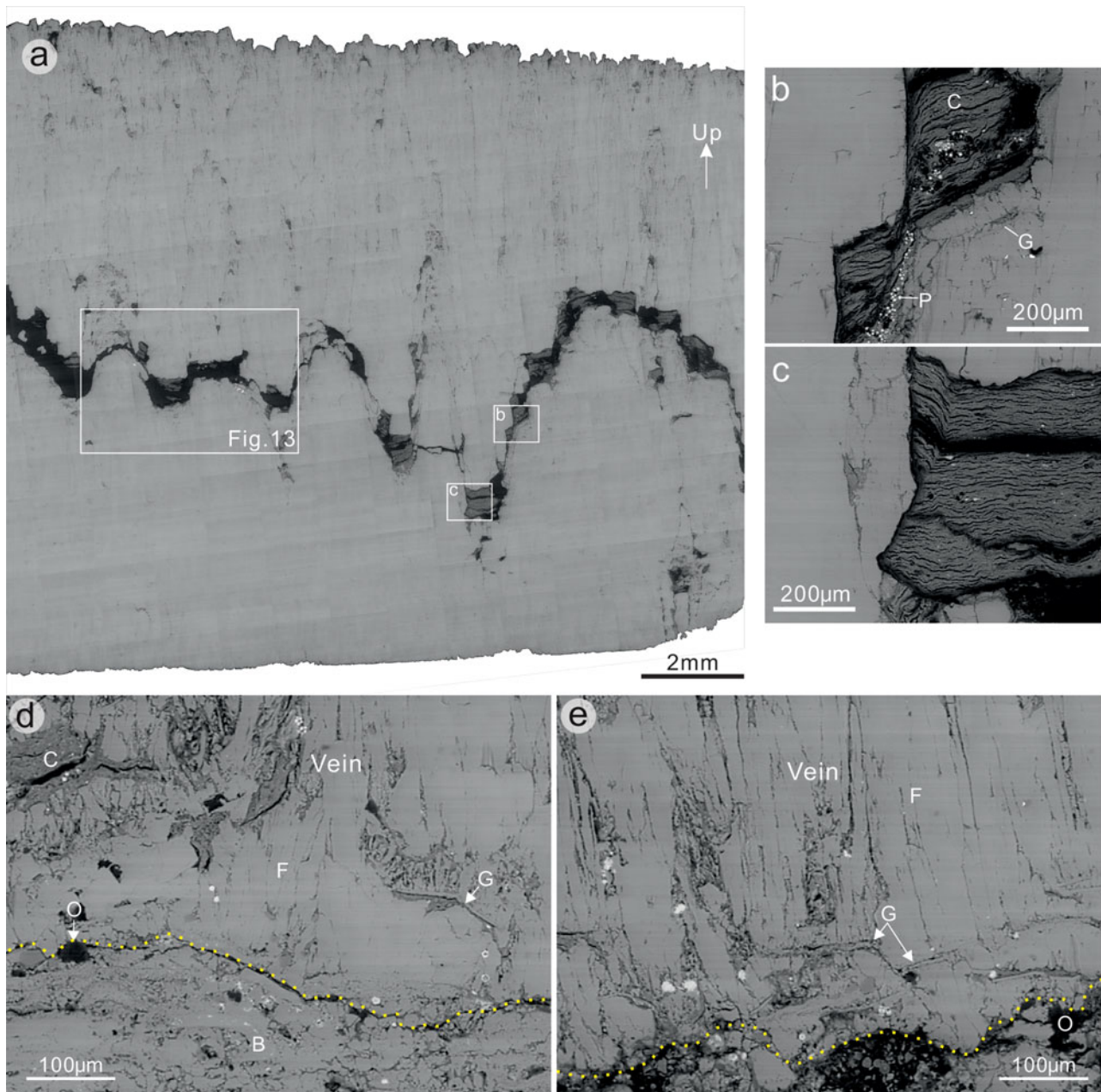
Figure 9. (Colour online) SEM backscattered electron images showing representative microstructures of fibrous calcite veins. (a) A bedding-parallel calcite vein consisting of a wavy median zone with insoluble residues of shale fragments, pyrite microcrystals and organic matter. The enlarged areas show (b) shale fragments along the steep flank of a column and (c) in a trough of a column. Note that the shale laminations are generally horizontal; however, the segments contacting uneven crystal faces are folded and parallel to the crystal faces. (d, e) Ghosts of bivalve fragments within bedding-parallel calcite veins. Note that the bivalve fragments are mostly subhorizontal and normal to calcite fibres, whereas some fragments are gently or steeply inclined. B – bivalve; C – clay; F – fibre; G – ghost of bivalve fragments; O – organic matter; P – pyrite.
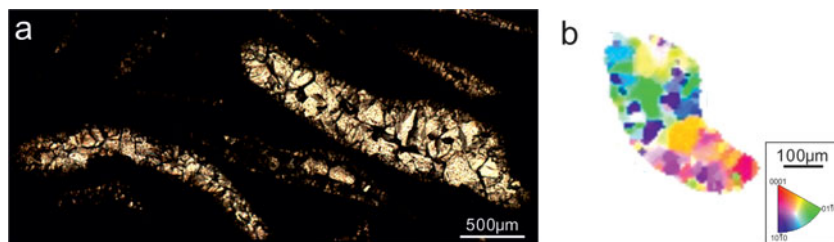

Figure 10. (Colour online) (a) Photomicrograph showing the cement of sparry calcite filling shell remains. Cross-polarized light. (b) Inverse pole figures (along *y* direction) showing crystallographic orientations of sparry calcite in a fossil mould.
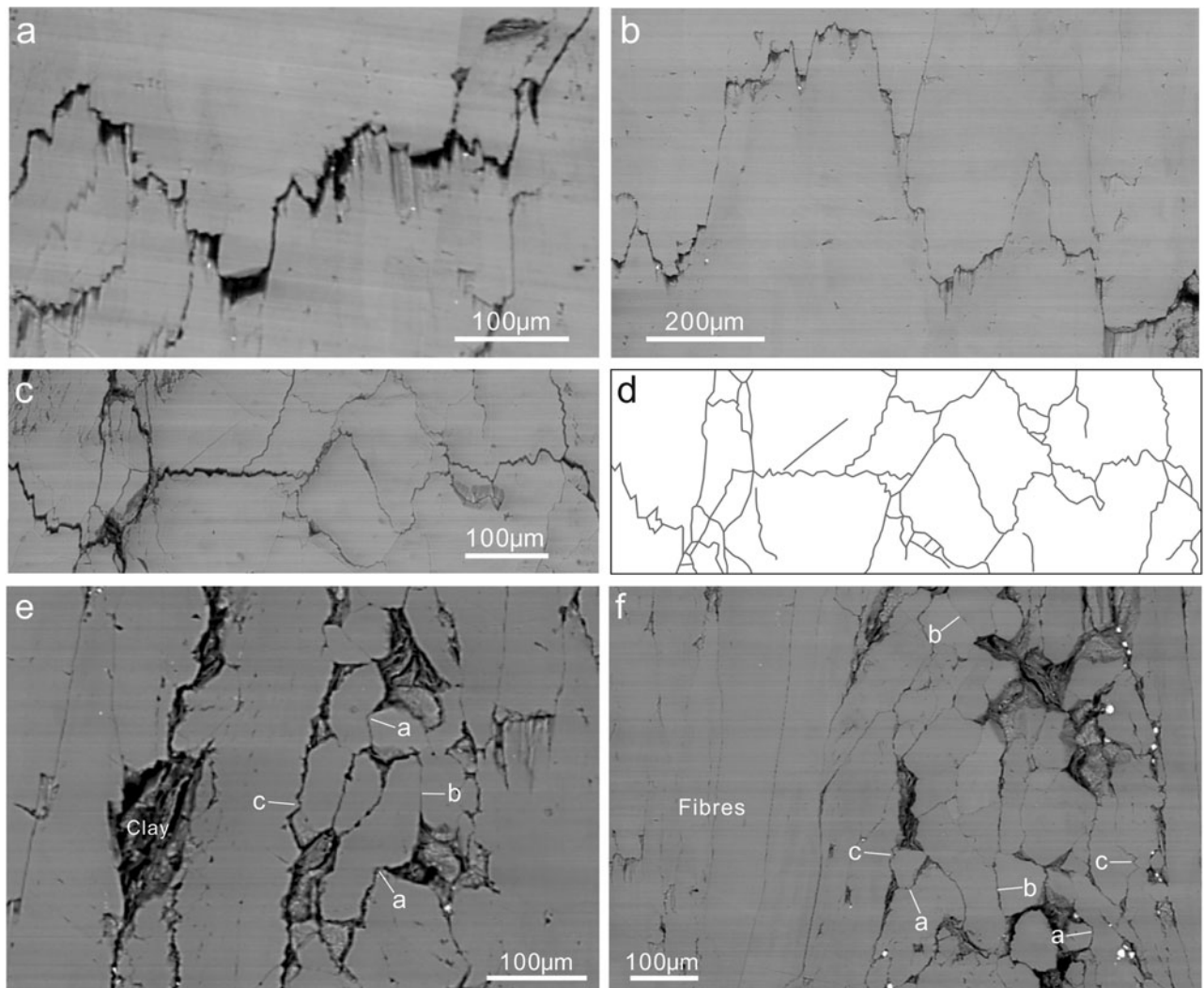
Figure 11. Pressure-solution features within fibrous calcite veins. (a) A microstylolite defined by a thin seam of organic matter with a maximum thickness of 17.5 µm. (b) A thin microstylolite exhibiting a composite fabric. (c) Interconnecting microstylolites exhibiting a fitted fabric. (d) Line-drawing traces of stylolites shown in (c). (e, f) Varied grain-contact styles in bedding-parallel calcite veins. Note that the larger fibres exhibit smooth crystal boundaries and lack evidence for pressure solution. a – indenting contact; b – truncating contact; c – interpenetrating contact.

6.b. Microstylolites

Microstylolites are commonly observed in the calcite veins, and truncate calcite crystals (Fig. 11). These microstylolites can be identified by wavy seams of organic matter with a maximum thickness of 22 µm (Fig. 11a, b). The microstylolites are generally subhorizontal; however, most veins contain inclined or even vertical segments. Some microstylolites occur as interconnecting networks, consisting of multiple stylolites in varying orientations that do not crosscut each other (Fig. 11c, d). These microstylolite networks mainly appear in closely packed aggregates of relatively small crystals with insoluble inclusions along crystal boundaries, exhibiting a fitted fabric. Unlike macrostylolites, single microstylolites either have sharp peaks or are composites of wavy or rectangular fragments with minor jagged surfaces. The amplitude of single columns ranges over 1–115 µm.

6.c. Grain contacts

The small, equant calcite grains within the calcite veins have different shapes and radii. Neighbouring grains in contact exhibit grain surface solution textures (Fig. 11e, f). The grains with the smaller radius of curvature commonly penetrate into the grain with the larger radius of curvature, resulting in an indenting grain contact as the most common type of grain contacts. Neighbouring grains with similar radii often exhibit flat contacts, which are identified as truncating grain contacts. Interpenetrating grain contacts, that is, mutually interlocking protrusions of grains into each other, were also observed. The sutured grain boundaries exhibit a similar morphology to microstylolites. In contrast to the equant grains, the vertical calcite fibres predominantly have smooth fibre boundaries, lacking signs of solution textures on grain surfaces (Fig. 11f).
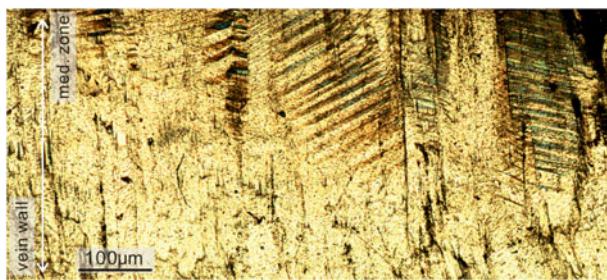
Figure 12. (Colour online) Photomicrograph showing the localized distribution of deformation twins in bedding-parallel calcite veins. Note that twins are absent from the outer part of the vein. Cross-polarized light.

6.d. Deformation twins

Intracrystalline deformation by twinning was observed to be concentrated along the stylolites in the calcite veins (Fig. 12). The deformation twins gradually disappear towards vein walls. This suggests that the twins formed during the early stage of fibre growth as growth twins, rather than deformation twins formed due to the loading of tectonic stress. Otherwise, the distribution of twins would be expected to be more homogeneously distributed within the veins. The twin sets often exhibit an interfingering pattern. Because the maximum principal stress σ_1 is ideally at about 45° to the glide plane (Lacombe, 2010; Fossen, 2016), the interfingering twins suggest a subvertical σ_1 that was responsible for creating those twins.

7. C-axis fabrics

EBSD results demonstrate that the equant calcite crystals along the stylolites predominantly exhibit random c-axis orientations (Fig. 13a–c), whereas the much larger fibres exhibit a preferred c-axis orientation in the subvertical direction (Fig. 13a, b, d). Some fibres with a medium plunge (e.g. fibres 4 and 5 in Fig. 13a) are commonly overgrown by neighbouring fibres. Those fibres have a tapering tip pointing towards vein walls. The steeply plunging calcite fibres tend to have a constant crystal width during growth, which is greater than low–medium plunging calcite fibres or equant grains. In contrast to the fibres, the sparry calcite cement filling skeletal fragments exhibit random c-axis orientations, and similar crystal sizes to those in vein stylolites (Fig. 10b).

8. Discussion

8.a. Diagenetic environment

Previous studies have demonstrated that local dissolution of bioclasts ($\delta^{13}C \approx 0 \permil$) could provide carbonate for the precipitation of calcite in veins (Marshall, 1982; Wolff, Rukin & Marshall, 1992; Meng, Hooker & Cartwright, 2017a). The carbon isotope values of bedding-parallel calcite veins (–0.5 to 1.8 ‰) presented in this study fall within a similar range to those of

their host rocks (Figs 6–8). The approximately equal values of $\delta^{13}C$ of calcite veins, shales and limestones could then suggest that the veins largely derived their carbonates from the host sediments. The source of the calcite could be neomorphic calcite provided by aragonitic fossils or sparry calcite cements filling pore spaces, or a combination of both. The prevalent aragonitic shells in the limestone and shale beds of the Stair Hole Formation, especially those embedded on vein surfaces and also within the veins (Figs 5b, c, 9d, e), could have released abundant carbonate for the growth of adjacent veins. This is because aragonite, as a more soluble polymorph of calcium carbonate, is metastable and readily transforms to calcite during burial (Maliva & Dickson, 1992; Hendry, Ditchfield & Marshall, 1995). In particular, the calcite veins and their host shales in beds 191, 193, 205, 215 and 219 share similar ranges of $\delta^{13}C$ values, suggesting that the veins were self-sourced by their host shales. It is notable that the unlithified aragonitic shell beds exhibit relatively more positive carbon isotope compositions, for example beds 194, 198 and 206 (Fig. 6). This could help to explain the higher $\delta^{13}C$ values of calcite veins in shale beds 205, 215 and 219, because the carbonate mineralogy in these beds predominantly consists of unlithified skeletal aragonite as the carbonate source for the calcite veins in the beds.

Organically derived bicarbonate with depleted ^{13}C ($\delta^{13}C \approx -25 \permil$ PDB) has been suggested as an alternative source for calcite veins, through *in situ* decomposition of organic matter under sulphate-reducing conditions (Hudson, 1978; McLane, 1995). Although the dark shales in the Stair Hole Formation is organic rich, the carbon isotope compositions of the calcite veins are not compatible with those infilled with organically derived carbonate. Moreover, the calcite veins presented in this study are mainly composed of ferroan calcite (El-Shahat & West, 1983), similar to that of neighbouring compacted biosparrudite. Ferroan calcite could not have been readily precipitated while SO_4^{2-} was present and transformed to S^{2-} and H_2S, indicating that the precipitation of ferrous calcite for the calcite veins and calcite cements of the compacted biosparrudite post-dated the process of bacterial sulphate reduction.

The oxygen isotope composition of carbonates is a function of the isotope composition and temperature T (°C) of the water in which the carbonate minerals were precipitated (Boggs, 2009). This relationship is determined by:

$$T = 16.9 - 4.2\,(\delta_c - \delta_w) + 0.13(\delta_c - \delta_w)^2 \qquad (1)$$

where δ_c is the equilibrium oxygen isotope composition of calcite and δ_w is the oxygen composition of the water from which the calcite was precipitated. The oxygen isotope composition therefore becomes more negative as the burial depth and temperature increases. The $\delta^{18}O$ values of the unlithified aragonitic shell beds 194 and 198 are *c.* 0 ‰ PDB (Fig. 6), suggesting that the seawater had an original oxygen isotope
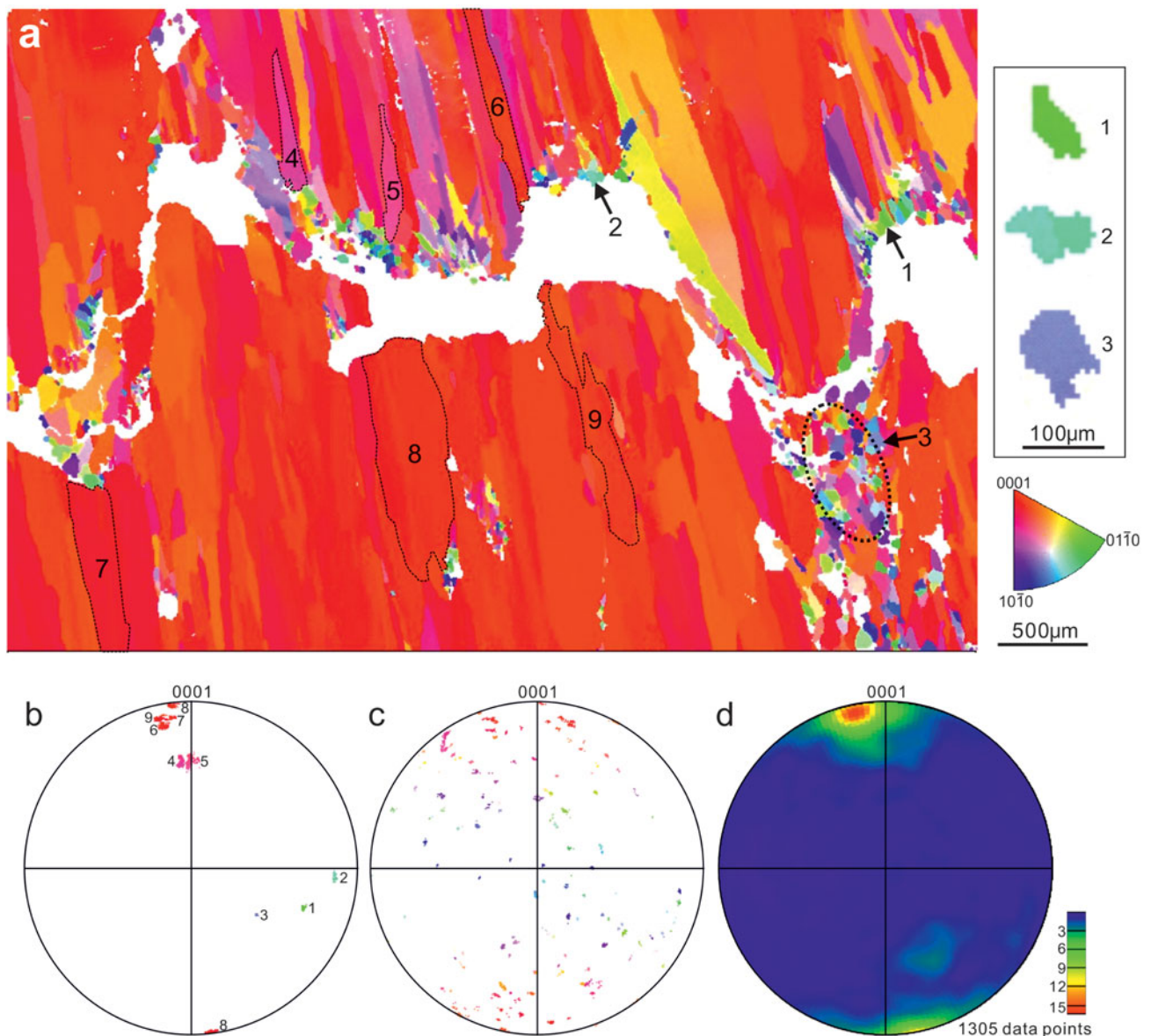
Figure 13. (Colour online) (a) Inverse pole figure (along *y* direction) showing the crystallographic preferred orientations (CPO) of a representative calcite vein (*y* direction is vertical). See sample location in Figure 9a. (b) Stereonet projections of c-axis pole orientations of the selected calcite crystals in the vein presented in (a). Lower hemisphere. The number of data points for grains 1–9 are 78, 110, 181, 1366, 1329, 2786, 4237, 10770 and 4589, respectively. (c) C-axes poles of the equant calcite crystals in the circular area of (a). 5283 data points. (d) Contoured plot of c-axis pole orientations of 1305 calcite crystals larger than 104 μm² in area. One data point per crystal.

composition of approximately zero per mil. If we assume that the diagenetic fluids for the calcite veins only consist of original seawater, from Equation (1) the formation temperature of the calcite veins would be *c.* 52.3–53.2 °C when given a $\delta^{18}O$ value of –5 to –6 ‰ PDB. However, the calculated temperatures are too high to be compatible with the palaeotemperature indicators of apatite fission track and vitrinite reflectance data reported in previous studies (Fig. 14) (Bray, Duddy & Green, 1998; Greenhalgh, 2016). This indicates that the diagenetic fluids from which calcite was precipitated could have more negative oxygen isotope compositions, and contain ^{18}O-depleted water constituents. Such porewater constituents are mostly

likely isotopically light meteoric waters: it has been suggested that the precipitation of ferran calcite cement for the compacted biosparrudites, which exhibit similar oxygen isotope ranges to the calcite veins, occurred as a typical phreatic process (Richter & Fuchtbauer, 1978). The mixing of seawater and isotopically light meteoric waters would affect the overall $\delta^{18}O$ signatures of the calcite precipitates. It should also be noted that evaporation may have occurred and caused a heavier isotope composition, although this effect is less likely to be a factor in a deep environment and also in a closed system.

In summary, the bedding-parallel calcite veins were mainly sourced by the host shales during burial, and
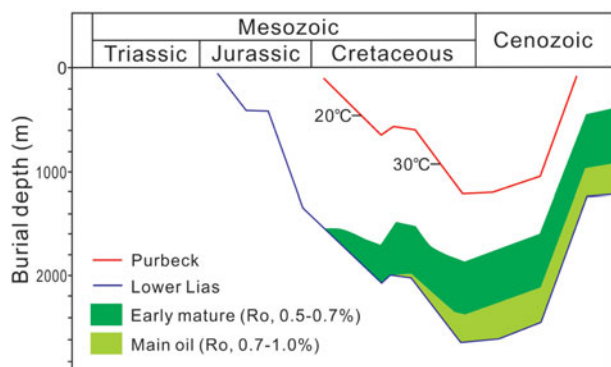
Figure 14. (Colour online) Burial curve and thermal history of the Purbeck Group and the Lower Lias Group. Data derived from Kimmridge-5 well in Dorset. Modified from Greenhalgh (2016).

post-date bacterial sulphate reduction. Calcite was precipitated from pore waters, which were a mixing of the original seawater and ^{18}O-depleted meteoric waters.

8.b. Vein generation and the palaeostress states

The stylolites (Figs 3b, c, 9a), microstylolites (Fig. 11a–d) and grain contact styles (Fig. 11e–f) found within the calcite veins suggest that pressure solution commenced during chemical compaction of their host sediments. The onset of chemical compaction has been suggested to occur at some point between 200 and 1500 m burial depth (Boggs, 2009; Goulty, Ramdham & Jones, 2012). Based on the burial history of the Durlstone Formation (Fig. 14), it is suggested that the calcite veins formed during burial and diagenesis, that is, chemical compaction, of the host sediments. Coupled with evidence from the predominant horizontal directions of stylolites and the interfingering twins in the calcite fibres (Fig. 12), it is inferred that the vertical compressional stress leading to pressure solution is the gravitational stress due to the overburden load.

The small, equant calcite crystals along the stylolites within calcite veins (Figs 11e, f, 13a) are similar to the sparry calcite filling shell moulds (Fig. 10), regarding crystal morphologies, sizes, crystallographic orientations and contact styles. Given the common coexistence of ghosts of bivalve fragments (Fig. 9d, e), those equant calcite in veins are interpreted to result from neomorphism of skeletal aragonite. The stylolites, as the vein initiation sites, could have formed due to pressure solution of neomorphic calcite within the horizons where aragonitic shells are concentrated when the neomorphic calcite grains became large enough to make contact with neighbouring grains. The stylolites generally lie in the horizontal direction with columns aligned vertically due to the lithostatic stress (overburden load).

The most commonly advocated mechanism to explain the genesis of fibrous calcite veins is that of overpressure triggered by primary oil migration from

thermally matured organic matter (Stoneley, 1983; Parnell & Carey, 1995; Parnell *et al.* 2000; Cobbold & Rodrigues, 2007; Rodrigues *et al.* 2009; Zanella *et al.* 2015; Hooker *et al.* 2017). This is theoretically possible because: (1) fluid pressure can hold apart fracture walls, and create dilational sites for the precipitation of calcite crystals when fluid pressure exceeds the sum of the minimum principal stress and the tensile strength of the shales (Stoneley, 1983); and (2) liquid oil has been observed within fluid inclusions in horizontal calcite veins (e.g. Parnell, Carey & Monson, 1996; Parnell *et al.* 2000). However, this mechanism is considered unlikely for the fibrous veins of the Stair Hole Member for a number of reasons.

Firstly, it has been suggested that the black Cretaceous shales as well as the underlying Kimmeridge Clay Formation are too immature to generate oils (Fig. 14) (Scotchman, 1987, 1989; Underhill & Stoneley, 1998). Oil inclusions were not found within the calcite veins, so there is no direct evidence that overpressure could have developed as a result of hydrocarbon generation. Secondly, overpressure could retard or completely shut down chemical compaction, because the elevated pore fluid pressures would reduce stresses at grain contacts and hence inhibit the production of stylolites (Scholle, 1977; Pittman & Larese, 1991; Paxton *et al.* 2002). Moreover, the extremely narrow spacing of the horizontal veins in Bed 219 of the Chief Beef Bed (Figs 3a, c, e, 4) may not favour a formation mechanism of hydraulic fracturing. According to fracture mechanics, the thickness of parallel horizontal hydrofractures is determined by (Mandl, 2005):

$$\frac{\delta d}{d} = \frac{1 - v^2}{E} (p - \sigma_v) \qquad (2)$$

where δd is fracture thickness; d is the distance between the mid-planes of neighbouring fractures; v is the Poisson's ratio; E is Young's modulus; p is pore fluid pressure; and σ_v is overburden stress. The average fracture thickness of single fractures δd_{av} from the fluid injection point to the fracture tip can be determined by:

$$\delta d_{av} = 3.14 \frac{1 - v^2}{E} (p - \sigma_v) L \qquad (3)$$

where L is the fracture length. Combing Equations (2) and (3), the approximation of the fracture spacing can be determined by:

$$d \approx 3L. \qquad (4)$$

Such a relationship between vein spacing and length is apparently not compatible with the calcite veins present in this study. Nevertheless, the condition that $d << 3L$ may still occur, but only if the veins formed by crack-seal processes (Ramsay, 1980). However, the critical evidence for crack-seal events (i.e. inclusion trails and bands) was not observed in the veins. Furthermore, if we assume that all veins have an equal growth rate, and thicker veins formed earlier than thinner veins, the nucleation of new hydrofractures would

preferentially occur along the interfaces between pre-existing calcite-filled veins and the host rocks because of the weak bonding between them (Bons & Montenari, 2005). It is therefore difficult to explain why new hydrofractures would have nucleated in horizons adjacent to the earlier veins rather than taking advantage of the weak planes of pre-existing vein-walls, especially in the case of neighbouring veins with a spacing of < 1 cm (Fig. 3e). However, in contrast, such a narrow spacing of veins can lend support to the role of pressure solution, because a decrease in bulk permeability induced by pressure solution favours a narrow spacing of parallel veins, as suggested in the cnoidal waves theory used for explaining the spacing of rhythmic bands in zebra dolomite (Kelka *et al.* 2017).

In summary, pressure solution during burial of the host sediments is suggested to have promoted the development of bedding-parallel calcite veins, which was facilitated by a vertical maximum compressive stress due to the overburden load.

8.c. Relationship between vein fabrics and vein growth process

In contrast to the calcite fibres, the calcite grains localized along the stylolites within calcite veins exhibit three main characteristic features revealed by our petrographic observations and EBSD measurements: (1) they have much smaller crystal sizes than the fibres; (2) they exhibit random c-axis orientations; and (3) pressure solution commonly occurs at interpenetrating or sutured grain contacts. These grains are similar to the sparry calcite filling fossil moulds (Fig. 10), and are regarded as early cement filling pore spaces in the shale matrix. Because stylolites have been suggested to be a major cement source in carbonate rocks (e.g. Hudson, 1975; Finkel & Wilkinson, 1990; Heydari, 2000), the stylolites within the calcite veins could have provided carbonates for the growth of calcite fibres, given the fact that the vein fibres grew from the stylolites towards the host rock. After mechanical compaction had essentially been completed and a stable grain framework had been established, dissolution of calcite could have largely occurred at grain contacts of the small equant calcite grains, as revealed by the prevalent pressure-solution features. These grains are more readily dissolved during chemical compaction, possibly because: (1) a mixture of grain sizes will lead to preferential dissolution of finer grains (Weyl, 1959); or (2) preferential dissolution of calcite grains would occur where their c-axes were not perpendicular to bedding, as calcite is most stable *in situ* with c-axes parallel to the direction of the maximum principal stress (Kamb, 1959; O'Brien *et al.* 1993), that is, vertical in the present study (Fig. 15). The dissolved carbonates would then have been transported through pore spaces to the sites for precipitation from pore waters.

Considering the low permeability of shales, it is more likely that solutes of calcite were transported
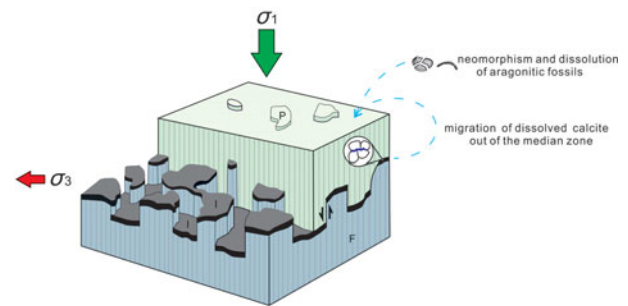

Figure 15. (Colour online) Simplified sketch illustrating the three-dimensional geometry and texture of bedding-parallel fibrous calcite veins. Modified from Railsback (2002). The enlarged area shows the pressure-solution sites where equant, sparry crystals are concentrated. Those sparry crystals may release calcite for increments of the outer fibres during pressure solution. F – fibre; I – insoluble minerals; P – protrusion.

by diffusion. The diffusive transfer could also be enhanced by the clay grains filling the stylolites and intergranular spaces because a clay film, consisting of multiple clay platelets with associated fluid films (Fig. 9b, c), could provide numerous diffusion paths (Renard *et al.* 2001).

The calcite fibres exhibit a continuity during growth and preferred subvertical c-axis orientations normal to bedding. This indicates that such c-axis orientations are more resistant to the overburden load. From the perspective of the thermodynamic theory of equilibrium under non-hydrostatic stress, the preferred c-axis orientation of calcite, as the weakest axis, tends to align with the maximum principal stress σ_1 (Kamb, 1959) when recrystallization occurs by solution and redeposition, in order to minimize the chemical potential required for equilibrium across the plane normal to the σ_1 axis. Calcite fibres with subvertical c-axes can therefore grow preferentially, whereas the others would be overgrown by fibres.

The calcite fibres exhibit two types of growth: (1) displacive growth, that is, surrounding shales have been displaced by calcite veins to accommodate their expansion; and (2) volume-for-volume replacive growth, that is, calcite fibres protrude into the contacting limestone beds, causing dissolution of the host limestones and re-precipitation of calcite on vein surfaces with an equal volume (Fig. 5). Both processes have been suggested to be controlled by the force of crystallization (Weyl, 1959). Although vein-displacive growth would be expected to be accompanied with vertical displacement of the surrounding shales, the volume of the bulk rock did not necessarily increase (Selles-Martinez, 1996); instead, shale beds could have been shortened during fibre growth. This is because the dissolution of aragonite and sparry calcite and re-deposition of calcite could have maintained the solid volume balance while the pore volume was reduced during the process of chemical compaction. The volumetric expansion of bedding-parallel veins could therefore have been established by redistribution

of carbonates in the hosts, and led to further bedding compaction.

Replacive growth of calcite fibres, which is represented by the irregular depressions on limestone planes and corresponding fibre protrusions, can only be observed at vein–limestone contacts (Fig. 5) because the authigenic calcite is incapable of mechanical displacement of the host limestones. The force of crystallization by growing calcite fibres exerted on the contacting limestones would result in an increase in the Gibbs free energy and hence a higher solubility of the hosts. This would produce a new dynamic equilibrium, in which authigenic calcite grew inwards into the host phase. In particular, the truncated ghosts of fossil fragments in biosparrudite, bounding calcite veins and limestones are typical representatives of vein-replacive features. Moreover, the similar values of carbon isotope compositions of neighbouring limestone beds and calcite veins (e.g. beds 205 and 206) could further suggest that the veins have derived their carbonates from the contact zone with the limestone beds by pressure solution arising from the force of crystallization controlled.

In summary, the petrographic and geochemical evidence presented overwhelmingly suggests that calcite fibres with subvertical c-axes grew preferentially due to the overburden load. The fibres exhibit a displacive growth in porous shales and a replacive growth at vein–limestone contacts, both phenomena ultimately controlled by the force of crystallization.

9. Conclusions

(1) The fibrous calcite veins in black shales (Cretaceous, southern UK), with $\delta^{13}C$ compositions of around zero per mil, derived carbonates mainly from the host rock. Pore fluids, from which calcite was precipitated, were a mixture of the original seawater and ^{18}O-depleted meteoric waters.

(2) Pressure solution, which is evident from stylolites, microstylolites and grain contact styles, occurred in the calcite veins. Pressure solution of sparry calcite as pore-filling cements is interpreted to have promoted the development of bedding-parallel calcite veins as a positive feedback mechanism during early burial of the sediments. Neomorphic calcite in the host shales and dissolved calcite from vein initiation localities could serve as carbonate sources for subsequent fibre growth.

(3) Calcite fibres exhibit a displacive growth in porous shales and a replacive growth at vein–limestone contacts, indicating the driving force of crystallization pressure of calcite.

(4) CPO patterns of calcite fibres could form as a response to the overburden pressure as the maximum principal stress during vein expansion.

(5) This study suggests that pressure solution could cause the formation of bedding-parallel calcite veins in black shales, especially those with a low organic maturity.

References

AL-AASM, I., CONIGLIO, M. & DESROCHERS, A. 1995. Formation of complex fibrous calcite veins in Upper Triassic strata of Wrangellia Terrain, British Columbia, Canada. *Sedimentary Geology* **100**, 83–95.

ANDREWS, J. E. & WALTON, W. 1990. Depositional environments within Middle Jurassic oyster-dominated lagoons: an integrated litho-, bio- and palynofacies study of the Duntulm Formation (Great Estuarine Group, Inner Hebrides). *Earth and Environmental Science Transactions of The Royal Society of Edinburgh* **81**, 1–22.

BARON, M. & PARNELL, J. 2007. Relationships between stylolites and cementation in sandstone reservoirs: Examples from the North Sea, UK and East Greenland. *Sedimentary Geology* **194**, 17–35.

BJORKUM, P. A. 1996. How important is pressure in causing dissolution of quartz in sandstones? *Journal of Sedimentary Research* **66**, 147–54.

BOGGS, S. 2009. *Petrology of Sedimentary Rocks*. Cambridge: Cambridge University Press.

BONS, P. D. 2000. The formation of veins and their microstructures. *Journal of the Virtual Explorer* **2**, doi: 10.3809/jvirtex.2000.00007.

BONS, P. D., ELBURG, M. A. & GOMEZ-RIVAS, E. 2012. A review of the formation of tectonic veins and their microstructures. *Journal of Structural Geology* **43**, 33–62.

BONS, P. D. & MONTENARI, M. 2005. The formation of antitaxial calcite veins with well-developed fibres, Oppaminda Creek, South Australia. *Journal of Structural Geology* **27**, 231–48.

BRAITHWAITE, C. 1989. Stylolites as open fluid conduits. *Marine and Petroleum Geology* **6**, 93–6.

BRAY, R. J., DUDDY, I. R. & GREEN, P. F. 1998. Multiple heating episodes in the Wessex Basin: implications for geological evolution and hydrocarbon generation. In *The Development, Evolution and Petroleum Geology of the Wessex Basin* (eds J. R. Underhill), pp. 199–213. Geological Society, London, Special Publication no. 133.

BRITISH GEOLOGICAL SURVEY. 2000. 1:63,360/1:50,000 geological map series, New Series, Sheet number 342 (East) and 343, Swanage. British Geological Survey, Keyworth.

BUXTON, T. M. & SIBLEY, D. F. 1981. Pressure solution features in a shallow burled limestone. *Journal of Sedimentary Research* **51**, 19–26.

CAROZZI, A. V. & VON BERGEN, D. 1987. Stylolitic porosity in carbonates: a critical factor for deep hydrocarbon production. *Journal of Petroleum Geology* **10**, 267–82.

CLEMENTS, R. 1993. Type-section of the Purbeck Limestone Group, Durlston Bay, Swanage, Dorset. *Proceedings of the Dorset Natural History and Archaeological Society* **114**, 181–206.

COBBOLD, P. R. & RODRIGUES, N. 2007. Seepage forces, important factors in the formation of horizontal hydraulic fractures and bedding-parallel fibrous veins ('beef' and 'cone-in-cone'). *Geofluids* **7**, 313–22.

COBBOLD, P. R., ZANELLA, A., RODRIGUES, N. & LOSETH, H. 2013. Bedding-parallel fibrous veins (beef and

cone-in-cone): Worldwide occurrence and possible significance in terms of fluid overpressure, hydrocarbon generation and mineralization. *Marine and Petroleum Geology* **43**, 1–20.

CONYBEARE, D. & SHAW, H. 2000. Fracturing, overpressure release and carbonate cementation in the Everest Complex, North Sea. *Clay Minerals* **35**, 135–49.

COSGROVE, J. W. 2001. Hydraulic fracturing during the formation and deformation of a basin: a factor in the dewatering of low-permeability sediments. *AAPG Bulletin* **85**, 737–48.

DEWERS, T. & ORTOLEVA, P. 1990. A coupled reaction/transport/mechanical model for intergranular pressure solution, stylolites, and differential compaction and cementation in clean sandstones. *Geochimica et Cosmochimica Acta* **54**, 1609–25.

EL-SHAHAT, A. & WEST, I. 1983. Early and late lithification of aragonitic bivalve beds in the Purbeck Formation (Upper Jurassic – Lower Cretaceous) of southern England. *Sedimentary Geology* **35**, 15–41.

EL-TABAKH, B. & WARREN, J. K. 1998. Origin of fibrous gypsum in the Newark rift basin, eastern North America. *Journal of Sedimentary Research* **68**, 88–99.

EVANS, M. A. 1995. Fluid inclusions in veins from the Middle Devonian shales: A record of deformation conditions and fluid evolution in the Appalachian Plateau. *Geological Society of America Bulletin* **107**, 327–39.

FINKEL, E. A. & WILKINSON, B. H. 1990. Stylolitization as source of cement in Mississippian Salem Limestone, west-central Indiana. *AAPG Bulletin* **74**, 174–86.

FITCHES, W., CAVE, R., CRAIG, J. & MALTMAN, A. 1986. Early veins as evidence of detachment in the Lower Palaeozoic rocks of the Welsh Basin. *Journal of Structural Geology* **8**, 607–20.

FLETCHER, R. C. & POLLARD, D. D. 1981. Anticrack model for pressure solution surfaces. *Geology* **9**, 419–24.

FOSSEN, H. 2016. *Structural Geology*. Cambridge: Cambridge University Press.

FOWLER, T. 1996. Flexural-slip generated bedding-parallel veins from central Victoria, Australia. *Journal of Structural Geology* **18**, 1399–415.

FOWLER, T. & WINSOR, C. 1997. Characteristics and occurrence of bedding-parallel slip surfaces and laminated veins in chevron folds from the Bendigo-Castlemaine goldfields: implications for flexural-slip folding. *Journal of Structural Geology* **19**, 799–815.

GOULTY, N., RAMDHAM, A. & JONES, S. 2012. Chemical compaction of mudrocks in the presence of overpressure. *Petroleum Geoscience* **18**, 471–9.

GREENHALGH, E. 2016. *The Jurassic Shales of the Wessex Area: Geology and Shale Oil and Shale Gas Resource Estimation*. London: British Geological Survey for the Oil and Gas Authority, 82 pp.

GUSTAVSON, T. C., HOVORKA, S. D. & DUTTON, A. R. 1994. Origin of satin spar veins in evaporite basins. *Journal of Sedimentary Research* **64**, 88–94.

GUZZETTA, G. 1984. Kinematics of stylolite formation and physics of the pressure-solution process. *Tectonophysics* **101**, 383–94.

HARA, H. & HISADA, K. I. 2007. Tectono-metamorphic evolution of the Cretaceous Shimanto accretionary complex, central Japan: Constraints from a fluid inclusion analysis of syn-tectonic veins. *Island Arc* **16**, 57–68.

HEAP, M. J., BAUD, P., REUSCHLE, T. & MEREDITH, P. G. 2014. Stylolites in limestones: Barriers to fluid flow? *Geology* **42**, 51–4.

HENDRY, J. P., DITCHFIELD, P. W. & MARSHALL, J. D. 1995. Two-stage neomorphism of Jurassic aragonitic bivalves: implications for early diagenesis. *Journal of Sedimentary Research* **65**, 214–24.

HEYDARI, E. 2000. Porosity loss, fluid flow, and mass transfer in limestone reservoirs: application to the Upper Jurassic Smackover Formation, Mississippi. *AAPG Bulletin* **84**, 100–18.

HILGERS, C. & URAI, J. L. 2005. On the arrangement of solid inclusions in fibrous veins and the role of the crack-seal mechanism. *Journal of Structural Geology* **27**, 481–94.

HILLIER, R. & COSGROVE, J. 2002. Core and seismic observations of overpressure-related deformation within Eocene sediments of the Outer Moray Firth, UKCS. *Petroleum Geoscience* **8**, 141–9.

HOOKER, J. N., CARTWRIGHT, J., STEPEHNSON, B., SILVER, C. R., DICKSON, A. J. & HSIEH, Y.-T. 2017. Fluid evolution in fracturing black shales, Appalachian Basin. *AAPG Bulletin* **101**, 1203–38.

HOPSON, P. M., WILKINSON, I. P. & WOODS, M. A. 2008. A stratigraphical framework for the Lower Cretaceous of England. Research Report RR/08/03, British Geological Survey, Keyworth.

HORTON, A. 1995. *Geology of the Country Around Thame*. Champaign: Balogh Scientific Books.

HOUSEKNECHT, D. W. 1984. Influence of grain size and temperature on intergranular pressure solution, quartz cementation, and porosity in a quartzose sandstone. *Journal of Sedimentary Research* **54**, 348–61.

HOUSEKNECHT, D. W. 1988. Intergranular pressure solution in four quartzose sandstones. *Journal of Sedimentary Research* **58**, 228–46.

HUDSON, J. 1975. Carbon isotopes and limestone cement. *Geology* **3**, 19–22.

HUDSON, J. 1978. Concretions, isotopes, and the diagenetic history of the Oxford Clay (Jurassic) of central England. *Sedimentology* **25**, 339–70.

HUMPHREYS, F. J. 2004. Characterisation of fine-scale microstructures by electron backscatter diffraction (EBSD). *Scripta Materialia* **51**, 771–6.

JAMISON, W. 2013. Bed-parallel expansion seams and shear surfaces in shales. Geoconvention 2013 (abstract), Calgary Canada, 6–12. http://www.searchanddiscovery.com/documents/2014/51053jamison/ndx_jamison.pdf.

JESSELL, M., WILLMAN, C. & GRAY, D. 1994. Bedding parallel veins and their relationship to folding. *Journal of Structural Geology* **16**, 753–67.

JOWETT, E. C. 1987. Formation of sulfide-calcite veinlets in the Kupferschiefer Cu-Ag deposits in Poland by natural hydrofracturing during basin subsidence. *The Journal of Geology* **95**, 513–26.

KAMB, W. B. 1959. Theory of preferred crystal orientation developed by crystallization under stress. *The Journal of Geology* **67**, 153–70.

KELKA, U., VEVEAKIS, M., KOEHN, D. & BEAUDOIN, N. 2017. Zebra rocks: compaction waves create ore deposits. *Scientific Reports* **7**, article no. 14260.

KOEHN, D. & PASSCHIER, C. W. 2000. Shear sense indicators in striped bedding-veins. *Journal of Structural Geology* **22**, 1141–51.

KOEHN, D., ROOD, M., BEAUDOIN, N., CHUNG, P., BONS, P. & GOMEZ-RIVAS, E. 2016. A new stylolite classification scheme to estimate compaction and local permeability variations. *Sedimentary Geology* **346**, 60–71.

LACOMBE, O. 2010. Calcite twins, a tool for tectonic studies in thrust belts and stable orogenic forelands. *Oil & Gas Science and Technology* **65**, 809–38.

LEHNER, F. K. 1995. A model for intergranular pressure solution in open systems. *Tectonophysics* **245**, 153–70.

Li, R., Dong, S., Lehrmann, D. & Duan, L. 2013. Tectonically driven organic fluid migration in the Dabashan Foreland Belt: Evidenced by geochemistry and geothermometry of vein-filling fibrous calcite with organic inclusions. *Journal of Asian Earth Sciences* **75**, 202–12.

Lindgreen, H. 1985. Diagenesis and primary migration in Upper Jurassic claystone source rocks in North Sea. *AAPG Bulletin* **69**, 525–36.

Machel, H. G. 1985. Fibrous gypsum and fibrous anhydrite in veins. *Sedimentology* **32**, 443–54.

Maher, H. D., Ogata, K. & Braathen, A. 2016. Cone-in-cone and beef mineralization associated with Triassic growth basin faulting and shallow shale diagenesis, Edgeøya, Svalbard. *Geological Magazine* **154**, 201–16.

Maliva, R. G. & Dickson, J. 1992. The mechanism of skeletal aragonite neomorphism: evidence from neomorphosed mollusks from the upper Purbeck Formation (Late Jurassic - Early Cretaceous), southern England. *Sedimentary Geology* **76**, 221–32.

Mandl, G. 2005. *Rock Joints*. Berlin: Springer.

Marshall, J. D. 1982. Isotopic composition of displacive fibrous calcite veins: reversals in pore-water composition trends during burial diagenesis. *Journal of Sedimentary Research* **52**, 615–30.

McLane, M. 1995. *Sedimentology*. Oxford: Oxford University Press.

Means, W. & Li, T. 2001. A laboratory simulation of fibrous veins: some first observations. *Journal of Structural Geology* **23**, 857–63.

Meng, Q., Hooker, J. & Cartwright, J. 2017a. Early overpressuring in organic-rich shales during burial: evidence from fibrous calcite veins in the Lower Jurassic Shales-with-Beef Member in the Wessex Basin, UK. *Journal of the Geological Society* **174**: 869–82.

Meng, Q., Hooker, J. & Cartwright, J. 2017b. Genesis of natural hydraulic fractures as an indicator of basin inversion. *Journal of Structural Geology* **102**, 1–20.

Meng, Q., Hooker, J. & Cartwright, J. 2018. Displacive widening of fibrous calcite veins: insights into force of crystallization. *Journal of Sedimentary Research* **88**, 327–43.

O'Brien, D. K., Manghnani, M. H., Tribble, J. S. & Wenk, H.-R. 1993. Preferred orientation and velocity anisotropy in marine clay-bearing calcareous sediments. In *Carbonate Microfabrics* (eds R. Rezak & D. L. Lavoie), pp. 149–61. Berlin: Springer.

Oldershaw, A. & Scoffin, T. 1967. The source of ferroan and non-ferroan calcite cements in the Halkin and Wenlock Limestones. *Geological Journal* **5**, 309–20.

Park, W. C. & Schot, E. H. 1968. Stylolites: their nature and origin. *Journal of Sedimentary Research* **38**, 175–91.

Parnell, J., Ansong, G. & Veale, C. 1994. Petrology of the bitumen (manjak) deposits of Barbados: hydrocarbon migration in an accretionary prism. *Marine and Petroleum Geology* **11**, 743–55.

Parnell, J. & Carey, P. F. 1995. Emplacement of bitumen (asphaltite) veins in the Neuquén Basin, Argentina. *AAPG Bulletin* **79**, 1798–815.

Parnell, J., Carey, P. & Monson, B. 1996. Fluid inclusion constraints on temperatures of petroleum migration from authigenic quartz in bitumen veins. *Chemical Geology* **129**, 217–26.

Parnell, J., Honghan, C., Middleton, D., Haggan, T. & Carey, P. 2000. Significance of fibrous mineral veins in hydrocarbon migration: fluid inclusion studies. *Journal of Geochemical Exploration* **69**, 623–7.

Paxton, S., Szabo, J., Ajdukiewicz, J. & Klimentidis, R. 2002. Construction of an intergranular volume compaction curve for evaluating and predicting compaction and porosity loss in rigid-grain sandstone reservoirs. *AAPG Bulletin* **86**, 2047–67.

Pittman, E. D. & Larese, R. E. 1991. Compaction of lithic sands: experimental results and applications. *AAPG Bulletin* **75**, 1279–99.

Radley, J. D. 2009. Archaic-style shell concentrations in brackish-water settings: Lower Cretaceous (Wealden) examples from southern England. *Cretaceous Research* **30**, 710–6.

Radley, J. D., Barker, M. J. & Munt, M. C. 1998. Bivalve trace fossils (Lockeia) from the Barnes High Sandstone (Wealden Group, Lower Cretaceous) of the Wessex Sub-basin, southern England. *Cretaceous Research* **19**, 505–9.

Railsback, L. B. 2002. An atlas of pressure solution features. http://www.gly.uga.edu/railsback/PDFintro1.html.

Ramsay, J. 1980. The crack-seal mechanism of rock deformation. *Nature* **284**, 135–9.

Renard, F., Dysthe, D., Feder, J., Bjorlykke, K. & Jamtveit, B. 2001. Enhanced pressure solution creep rates induced by clay particles: Experimental evidence in salt aggregates. *Geophysical Research Letters* **28**, 1295–8.

Renard, F., Gratier, J. P. & Jamtveit, B. 2000. Kinetics of crack-sealing, intergranular pressure solution, and compaction around active faults. *Journal of Structural Geology* **22**, 1395–407.

Renard, F., Ortoleva, P. & Gratier, J. P. 1997. Pressure solution in sandstones: influence of clays and dependence on temperature and stress. *Tectonophysics* **280**, 257–66.

Rezaee, M. R. & Tingate, P. R. 1997. Origin of quartz cement in the Tirrawarra sandstone, southern Cooper basin, South Australia. *Journal of Sedimentary Research* **67**, 168–77.

Richter, D. K. & Fuchtbauer, H. 1978. Ferroan calcite replacement indicates former magnesian calcite skeletons. *Sedimentology* **25**, 843–60.

Robinson, S. A. & Hesselbo, S. P. 2004. Fossil-wood carbon-isotope stratigraphy of the non-marine Wealden Group (Lower Cretaceous, southern England). *Journal of the Geological Society* **161**, 133–45.

Rodrigues, N., Cobbold, P. R., Loseth, H. & Ruffet, G. 2009. Widespread bedding-parallel veins of fibrous calcite ('beef') in a mature source rock (Vaca Muerta Fm, Neuquén Basin, Argentina): evidence for overpressure and horizontal compression. *Journal of the Geological Society* **166**, 695–709.

Rukin, N. 1990. The diagenesis of the Shales-with-beef of the Lower Lias, West Dorset. PhD Thesis, University of Liverpool. Published thesis.

Rutter, E. 1983. Pressure solution in nature, theory and experiment. *Journal of the Geological Society* **140**, 725–40.

Rutter, E. & Elliott, D. 1976. The kinetics of rock deformation by pressure solution. *Philosophical Transactions of the Royal Society of London A: Mathematical, Physical and Engineering Sciences* **283**, 203–19.

Schnyder, J., Ruffel, A., Deconinck, J.-F. & Baudin, F. 2006. Conjunctive use of spectral gamma-ray logs and clay mineralogy in defining late Jurassic–early Cretaceous palaeoclimate change (Dorset, UK). *Palaeogeography, Palaeoclimatology, Palaeoecology* **229**, 303–20.

SCHOLLE, P. A. 1977. Chalk diagenesis and its relation to petroleum exploration: oil from chalks, a modern miracle? *AAPG Bulletin* **61**, 982–1009.

SCOTCHMAN, I. 1987. Clay diagenesis in the Kimmeridge Clay Formation, onshore UK, and its relation to organic maturation. *Mineralogical Magazine* **51**, 535–51.

SCOTCHMAN, I. 1989. Diagenesis of the Kimmeridge Clay formation, onshore UK. *Journal of the Geological Society* **146**, 285–303.

SELLES-MARTINEZ, J. 1994. New insights in the origin of cone-in-cone structures. *Carbonates and Evaporites* **9**, 172–86.

SELLES-MARTINEZ, J. 1996. Concretion morphology, classification and genesis. *Earth-Science Reviews* **41**, 177–210.

SHEARMAN, D., MOSSOP, G., DUNSMORE, H. & MARTIN, M. 1972. Origin of gypsum veins by hydraulic fracture. *Institution of Mining and Metallurgy, Transactions, Section B: Applied Earth Science* **81**, 149–55.

SIBLEY, D. F. & BLATT, H. 1976. Intergranular pressure solution and cementation of the Tuscarora orthoquartzite. *Journal of Sedimentary Research* **46**, 881–96.

STEWART, D., RUFFELL, A., WACH, G. & GOLDRING, R. 1991. Lagoonal sedimentation and fluctuating salinities in the Vectis Formation (Wealden Group, Lower Cretaceous) of the Isle of Wight, southern England. *Sedimentary Geology* **72**, 117–34.

STONELEY, R. 1983. Fibrous calcite veins, overpressures, and primary oil migration. *AAPG Bulletin* **67**, 1427–8.

SUCHY, V., DOBES, P., FILIP, J., STEJSKAL, M. & ZEMAN, A. 2002. Conditions for veining in the Barrandian Basin (Lower Palaeozoic), Czech Republic: evidence from fluid inclusion and apatite fission track analysis. *Tectonophysics* **348**, 25–50.

TABER, S. 1918. The origin of veinlets in the Silurian and Devonian strata of central New York. *The Journal of Geology* **26**, 56–73.

TADA, R., MALIVA, R. & SIEVER, R. 1987. A new mechanism for pressure solution in porous quartzose sandstone. *Geochimica et Cosmochimica Acta* **51**, 2295–301.

TADA, R. & SIEVER, R. 1989. Pressure solution during diagenesis. *Annual Review of Earth and Planetary Sciences* **17**, 89–118.

THOMSON, A. 1959. Pressure solution and porosity. In *Silica in Sediments* (eds H. A. Ireland), pp. 92–111. Society of Economic Paleontologists and Mineralogists, Special Publication no. 7.

UNDERHILL, J. R. & STONELEY, R. 1998. Introduction to the development, evolution and petroleum geology of the Wessex Basin. In: *The Development, Evolution and Petroleum Geology of the Wessex Basin* (eds J. R. Underhill), pp. 1–18. Geological Society, London, Special Publication no. 133.

VANNUCCHI, P. 2001. Monitoring paleo-fluid pressure through vein microstructures. *Journal of Geodynamics* **32**, 567–81.

WATTS, N. 1978. Displacive calcite: evidence from recent and ancient calcretes. *Geology* **6**, 699–703.

WESTHEAD, R. & MATHER, A. 1996. An updated lithostratigraphy for the Purbeck Limestone Group in the Dorset type-area. *Proceedings of the Geologists' Association* **107**, 117–28.

WEYL, P. K. 1959. Pressure solution and the force of crystallization: a phenomenological theory. *Journal of Geophysical Research* **64**, 2001–25.

WILTSCHKO, D. V. & MORSE, J. W. 2001. Crystallization pressure versus "crack seal" as the mechanism for banded veins. *Geology* **29**, 79–82.

WOLFF, G. A., RUKIN, N. & MARSHALL, J. D. 1992. Geochemistry of an early diagenetic concretion from the Birchi Bed (L. Lias, W. Dorset, UK). *Organic Geochemistry* **19**, 431–44.

WORDEN, R. H., OXTOBY, N. H. & SMALLEY, P. C. 1998. Can oil emplacement prevent quartz cementation in sandstones? *Petroleum Geoscience* **4**, 129–37.

YASUHARA, H., ELSWORTH, D. & POLAK, A. 2003. A mechanistic model for compaction of granular aggregates moderated by pressure solution. *Journal of Geophysical Research: Solid Earth* **108**, doi: 10.1029/2003JB002536.

ZANELLA, A., COBBOLD, P. R. & BOASSEN, T. 2015. Natural hydraulic fractures in the Wessex Basin, SW England: widespread distribution, composition and history. *Marine and Petroleum Geology* **68**, 438–48.

ZANELLA, A., COBBOLD, P. R. & DE VESLUD, C. L. C. 2014. Physical modelling of chemical compaction, overpressure development, hydraulic fracturing and thrust detachments in organic-rich source rock. *Marine and Petroleum Geology* **55**, 262–74.

ZANELLA, A., COBBOLD, P. R., RUFFET, G. & LEANZA, H. A. 2015. Geological evidence for fluid overpressure, hydraulic fracturing and strong heating during maturation and migration of hydrocarbons in Mesozoic rocks of the northern Neuquén Basin, Mendoza Province, Argentina. *Journal of South American Earth Sciences* **62**, 229–42.